

## MAGNETOSTRUCTURAL STUDY OF NANOSTRUCTURED AND AMORPHOUS BULK ALLOYS $(\text{Co-P})_{100-x}\text{Cu}_x$

L. A. Kuzovnikova<sup>1\*</sup>, E. A. Denisova<sup>2,3</sup>,  
I. V. Nemtsev<sup>2,3,4</sup>, R. S. Iskhakov<sup>2</sup>,  
S. V. Komogortsev<sup>2</sup>, A. A. Kuzovnikov<sup>1</sup>,  
V. K. Maltsev<sup>2</sup>, and N. A. Shepeta<sup>3</sup>

The work reports a magnetostructural study of bulk nanostructured composite materials Co–P/Cu prepared by dynamic compaction (DC) and uniaxial cold pressing (CP). The initial particles with amorphous and crystalline structure are synthesized by chemical deposition. Magnetic characteristics of composites (saturation magnetization, Bloch constant, local anisotropy field, ferro-magnetic resonance line width, coercive force) are studied. The phase compositions of initial composite particles and compacts prepared by two methods (DC and CP) are determined from the anisotropy field and the Bloch constant values using magnetic phase analysis. It is shown that the use of composite particles in dynamic compaction allows obtaining homogeneous nanostructured bulk materials while preserving magnetic characteristics of initial powders.

**DOI:** 10.1134/S0022476621050164

**Keywords:** cobalt–copper composite material, chemical deposition, magnetic properties, amorphous bulk alloys, dynamic compaction.

### INTRODUCTION

Novel metallic materials prepared from materials with non-equilibrium meta-stable structures (nanoparticles, nanostructured powders, etc.) demonstrate an unusual combination of physical and chemical properties. High mechanical strength and corrosion resistance along with soft magnetic properties make them promising for the use in magnetic shielding, magnetic parts in valves, clutches or relays, numerous electrical devices such as electronic measurement and monitoring systems, magnetic wires, sensors, bandpass filters [1, 2]. Their practical use requires preparation of massive materials preserving the properties of nanostructured powders. The most common techniques include pressing in high vacuum, pressure sintering, hot isostatic pressing, severe plastic deformation, and high-temperature gas extrusion [3-5].

However, static compaction of powders meets a number of problems. Cold pressing does not always produce dense samples, while hot pressing is often associated with recrystallization and formation of large pores during the stage of high-temperature treatment. Shock wave methods are promising for the compaction of nanostructured powders. Dynamic methods

---

<sup>1</sup>Krasnoyarsk Transport Institute, Branch of the Federal State Budget Institution of Higher Education “Irkutsk State Transport University IrGUPS”, Krasnoyarsk, Russia; \*lund@mail.ru. <sup>2</sup>Kirensky Institute of Physics, Federal Research Center, Krasnoyarsk Science Center, Siberian Branch, Russian Academy of Sciences, Krasnoyarsk, Russia. <sup>3</sup>Siberian Federal University, Krasnoyarsk, Russia. <sup>4</sup>Federal Research Center Krasnoyarsk Science Center, Siberian Branch, Russian Academy of Sciences, Krasnoyarsk, Russia. Original article submitted October 23, 2020; revised December 3, 2020; accepted December 7, 2020.

of nanopowder compaction allow overcoming adhesive forces, especially important for nanoparticles with highly developed surfaces, to reach a higher density of compacted samples at the same pressure [6]. The material cools rapidly and the metastable phases are stabilized after the shock wave [7].

It was established earlier that optimal magnetic properties of bulk materials from Co based amorphous alloys are observed for certain relative arrangements and weight ratios of amorphous and microcrystalline phases [8], which can be achieved by varying explosive pressing regimes. It was shown that samples remain X-ray amorphous under shock wave loading (SWL) pressures  $P_1 < 3.2$  GPa. Hence, developing a non-destructive method of phase composition control for bulk amorphous or nanocrystalline alloys becomes an important task.

Our research is related to the preparation of bulk nanostructured materials by dynamic compaction (DC) of powders with core–shell composite particles Co(P)/Cu. The purpose of this work is to study the possibilities of nuclear magnetic resonance, magnetostructural and magnetic phase methods, along with commonly used methods such as electron microscopy combined with powder X-ray analysis, to characterize bulk nanostructured or amorphous cobalt based alloys.

## EXPERIMENTAL

Bulk Co–P/Cu samples were prepared by dynamic compaction (shock-wave loading) using flat pressing ( $P \sim 3.5$  GPa) and uniaxial static pressing in a hydrostatic press with a pressure varying from  $2 \cdot 10^5$  Pa to  $8 \cdot 10^5$  Pa. The initial powders for pressing were fine powders prepared from composite particles: a core of amorphous Co<sub>88</sub>P<sub>12</sub> (or crystalline Co<sub>95</sub>P<sub>5</sub>) alloy covered with copper. Powders (Co<sub>88</sub>P<sub>12</sub>)<sub>100-x</sub>/Cu<sub>x</sub> ( $x = 20\%, 50\%, 70\%$ ), (Co<sub>95</sub>P<sub>5</sub>)<sub>50</sub>/Cu<sub>50</sub> were obtained by combined chemical deposition by the reaction of metal reduction from aqueous solutions of the corresponding salts. First, fine powders of Co–P alloys (with particle size from 0.1  $\mu\text{m}$  to 1.3  $\mu\text{m}$ ) were prepared from aqueous solutions of the cobalt salt (CoSO<sub>4</sub>) ( $T = 80^\circ\text{C}$ ) using sodium hypophosphite (NaH<sub>2</sub>PO<sub>2</sub>) as the reducing agent [9]. It was established earlier in [10] that thus prepared powders of alloy Co<sub>88</sub>P<sub>12</sub> are amorphous while powders of alloy Co<sub>95</sub>P<sub>5</sub> are crystalline with a hexagonal close-packed (hcp) structure. Then the Co(P) alloy particles were covered with copper shells of various thicknesses. Copper was deposited by using formaldehyde as a reducing agent in the solutions for chemical coppering of Co(P) powders. It was established that the composite particles were spherical for all studied concentrations of phosphorus and copper, the copper layer thickness depended on copper content and varied from 0.05  $\mu\text{m}$  for Co(P)<sub>80</sub>/Cu<sub>20</sub> powders to 0.7  $\mu\text{m}$  for (Co–P)<sub>10</sub>/Cu<sub>90</sub> powders [11].

The structure, morphology, and phase composition of initial powders and compacts were studied by scanning electron microscopy (SEM) (HitachiTM 3000 with an energy dispersive accessory), X-ray diffraction (DRON-4, CuK $\alpha$  radiation), and nuclear magnetic resonance (NMR). The NMR spectra were recorded using the spin echo method. Low-temperature and field dependences of magnetization recorded on a vibration magnetometer in the field range from 0 kOe to 14 kOe at 77–300 K. The resonance characteristics were measured on a standard 9.2 GHz EPA-2M spectrometer. The samples for magnetization measurements were cut from the compacts in the form of 3  $\times$  7  $\times$  1 mm plane-parallel plates. The local anisotropy field  $H_a = 2K/M_s$  and the size of orientationally distinguished region of this anisotropy  $2R_C$  were calculated from magnetization curves before saturation  $M(H)$  [12] measured on a vibrating sample magnetometer in the field range up to 14 kOe. The phase composition of the ferromagnetic alloy was estimated by measuring the magnetization dependence on temperature and external field [13].

## RESULTS AND DISCUSSION

The samples after dynamic compaction are 15  $\times$  8  $\times$  2 mm solid metal plates without visible cracks or pores. For a more detailed analysis, fractures and thin sections of compacted specimens were studied. Fig. 1 shows SEM images of bulk samples Co<sub>88</sub>P<sub>12</sub>/Cu prepared by DC (a), Co<sub>95</sub>P<sub>5</sub>/Cu samples prepared by cold pressing (CP) (c, d), histogram showing the

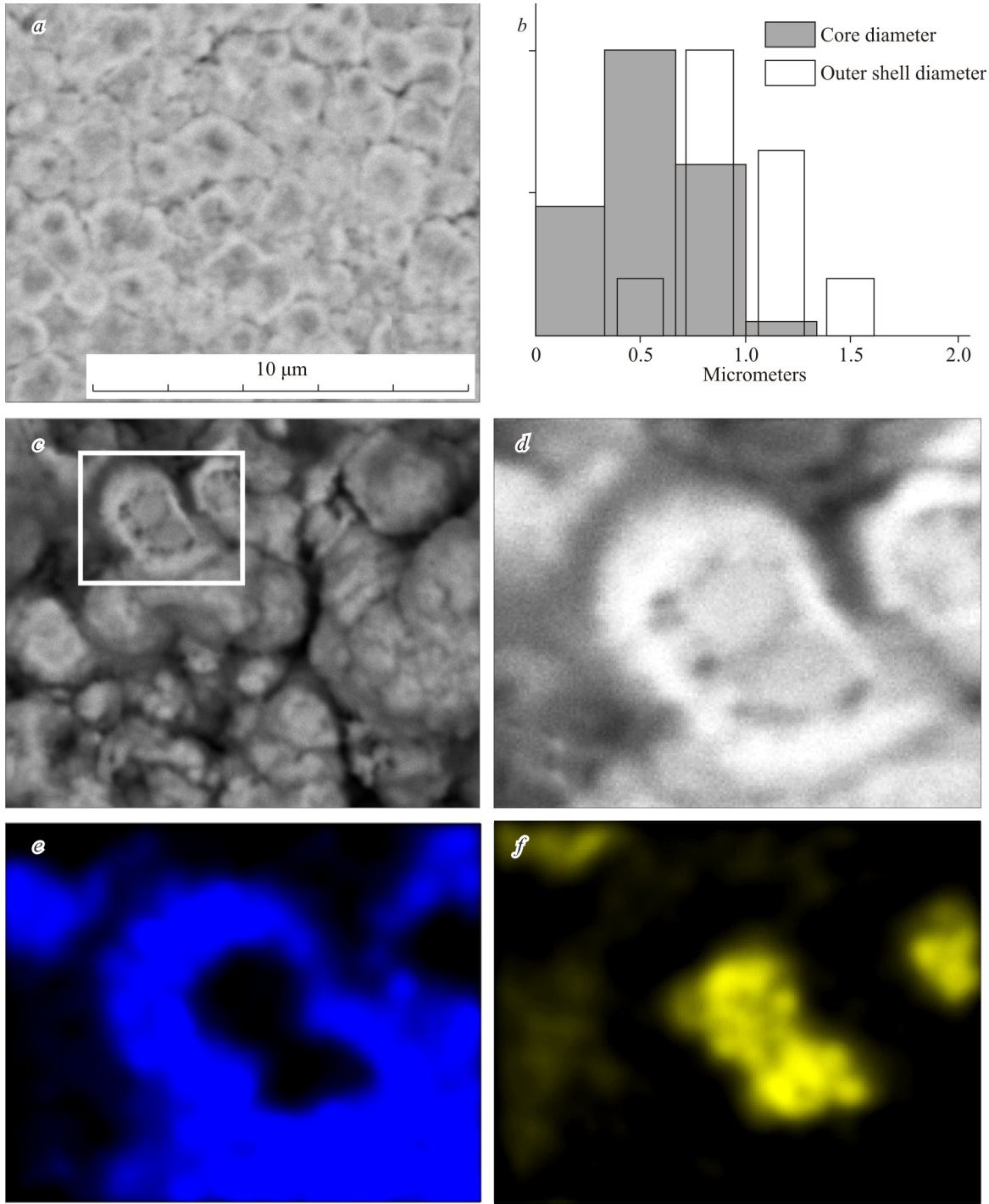


**Fig. 1.** SEM images of thin sections of Co<sub>88</sub>P<sub>12</sub>/Cu (*a*) and Co<sub>95</sub>P<sub>5</sub>/Cu (*c*, *d*) bulk samples; histogram showing the size distribution of composite particles (*b*); EDX maps of copper and cobalt distribution in the energy dispersive analysis (*e*, *f*).

size distribution of composite particles (*b*), and distribution maps for the elements (copper and cobalt) in the energy dispersive analysis (EDX) (*e*, *f*). As can be seen, the use of optimal DC modes allows preserving the core–shell structure in the compacts (dark and light regions correspond to Co(P) cores and to copper, respectively).

The diffraction patterns of composite particles and Co<sub>88</sub>P<sub>12</sub>/Cu compacts show reflections of the copper shell face-centered cubic lattice (fcc) and a weak amorphous halo in the 2θ region ~ 44.6° (Fig. 2). Such diffractograms signify that the

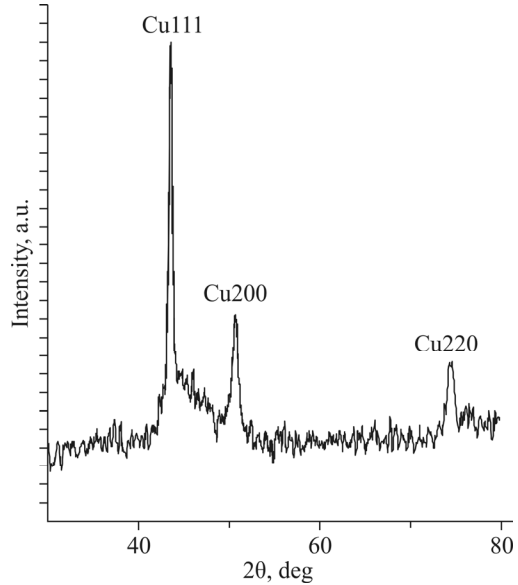


**Fig. 2.** Diffraction pattern of the bulk  $(\text{Co}_{88}\text{P}_{12})_{80}/\text{Cu}_{20}$  sample prepared by dynamic compaction.

particles of these powders are nanocrystalline or amorphous, and their phase composition cannot be determined unambiguously. The coherent scattering region estimated by the Scherrer equation varies within 20-100 nm, depending on the composition of the Co(P) alloy.

As is known, electron microscopy, with all its obvious advantages, probes only the surface of bulk samples. Therefore, a complex of magnetostructural and magnetic phase studies was used to retrieve additional information on the changes occurring in the immediate environment of Co and in the magnetic microstructure of composite particles during the compaction of Co(P)/Cu powders.

In recent decades, nuclear magnetic resonance has been widely employed to determine the structure and local magnetic properties of novel magnetic materials, particularly, cobalt multilayers and nanoparticles [14-16]. NMR spectra provide information on phase composition, certain crystal structures, number of various asymmetrical positions of the studied core, and magnetic structure of the sample. Fig. 3 shows the NMR spectra recorded at  $T = 77$  K for initial composite particles and compacts.

The width and shape of NMR spectra of initial particles and bulk samples of all compositions indicate that the ferromagnetic phase Co(P) has a heterophase structure: the signal is a superposition of several lines. The available experience in interpreting such spectra of cobalt alloys [17, 18] suggests that cobalt atoms with hcp and fcc types of immediate environment having different numbers of non-cobalt immediate neighbors give NMR lines at different frequencies. The NMR spectrum of pure cobalt at 77 K is characterized by two fundamental frequencies of 216 MHz for the fcc Co phase and 226 MHz for the hcp Co phase [19]. Replacing one Co atom in the nearest environment of 12 neighbors by copper or phosphorus leads to a 18 MHz low-frequency shift [17]. This rule was used to choose the line positions when decomposing the spectrum into components. It was found that a satisfactory description is achieved using three lines (Fig. 3): two lines corresponding to the Co fcc (with 12 Co atoms in the first coordination sphere and one cobalt atom substituted by phosphorus or copper, 216 MHz and 198 MHz, respectively) and one line corresponding to the Co hcp (with one substituted atom in the immediate environment of cobalt, 208 MHz). The intensities and widths of the lines were chosen using the least squares method.

Fitting the NMR spectra of composite powders  $(\text{Co}_{88}\text{P}_{12})_{100-x}/\text{Cu}_x$  by Gaussian curves showed that the area under the curve corresponding to Co atoms with a fcc immediate environment ( $S_{\text{fcc}}$ ) is almost 4-5 times larger than the area corresponding to the second NMR component with a hcp immediate environment ( $S_{\text{hcp}}$ ). The area ratio  $S_{\text{fcc}}/S_{\text{hcp}}$  is not sufficient to determine the sample's phase ratio quantitatively, which would require taking into account the amplification

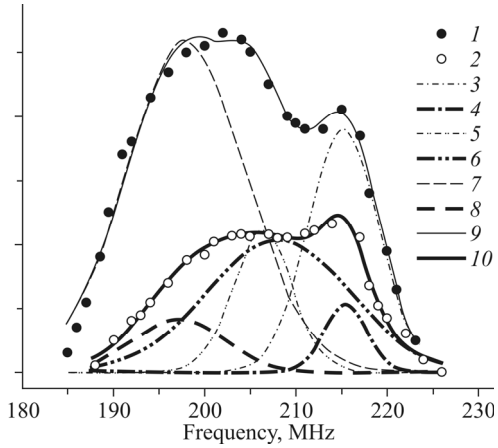


**Fig. 3.** NMR spectra measured at 77 K for initial  $(\text{Co}_{88}\text{P}_{12})_{80}/\text{Cu}_{20}$  (1) powders and the bulk sample prepared by dynamic compaction (2). Gaussian peak of Co with the fcc type of immediate environment (3, 4); Co fcc with one Co atom of the first coordination sphere substituted by copper or phosphorus (5, 6); Gaussian peak of Co with the hcp type of immediate environment (7, 8); sum of Gaussian peaks (9, 10) (for initial powders  $(\text{Co}_{88}\text{P}_{12})_{80}/\text{Cu}_{20}$  – 3, 5, 7, 9; for the bulk sample – 4, 6, 8, 10).

factor having different values for different phases. However, if the area ratio changes during various transformations, the phase ratio in the sample also changes. Comparing the ratio areas under the peaks corresponding to hcp and fcc phases (Fig. 3) in initial and compacted powders shows that the SWL during the compacting increases the number of cobalt atoms with the hcp type of immediate environment. The ratio of the number of atoms with hcp and fcc types of immediate environments is somewhat different in the compacts with different copper shell thicknesses. The content of cobalt atoms with the fcc symmetry of the nearest environment increases together with the copper content. It is known that Co(P) alloys prepared by reduction from solution contain also an amorphous phase along with crystalline hcp and fcc phases [13]. Note that the type of the immediate environment (fcc or hcp) determined by the NMR spectrum decomposition does not mean that the phase is crystalline. Thus, it was shown earlier that the immediate environment of Co atoms in the powders of Co(P) amorphous alloys belongs to the fcc type [18].

The saturation magnetization of initial composite powders decreases monotonically as the copper content increases from 800 G for  $\text{Co}_{88}\text{P}_{12}$  to 240 G for  $(\text{Co}_{88}\text{P}_{12})_{10}/\text{Cu}_{90}$ . The saturation magnetization and coercive force ( $H_C \sim 200$  Oe) values remain virtually unchanged after the compaction. It was found that magnetization curves measured at mutually perpendicular external field directions relative to the plate are almost coinciding, similarly to the ferromagnetic resonance (FMR) spectra recorded at different sample orientations relative to the external field. Therefore, in the case of bulk composite samples  $(\text{Co}_{88}\text{P}_{12})_{100-x}/\text{Cu}_x$ , the shape of the magnetization curve is not determined by the dipole-dipole interaction for all studied copper contents.

The approach to saturation curves show that magnetization curves agree well with Akulov's law  $M(H) = M_0(1 - aH_a^2 / H^2)$  ( $a$  is the symmetry coefficient and  $H_a = 2K/M_s$  is the local anisotropy field) in the region of large fields (above 5 kOe) for all  $x$  values of studied initial powders and compacts  $(\text{Co}_{88}\text{P}_{12})_x/\text{Cu}_{100-x}$  (Fig. 4).

As a result, it was possible to determine the magnitude of the local anisotropy field  $H_a$ . In the low-temperature region and up to 1/3 of the Curie temperature, the magnetization of ferromagnets is described by Bloch's law  $M(T) = M_0(1 - BT^{3/2})$ , where  $M_0$  is the saturation magnetization at 0 K. The Bloch constants for all studied samples were determined from the low-temperature measurements of saturation magnetization. Since the single-phase alloys Co(P) (hcp, fcc, and

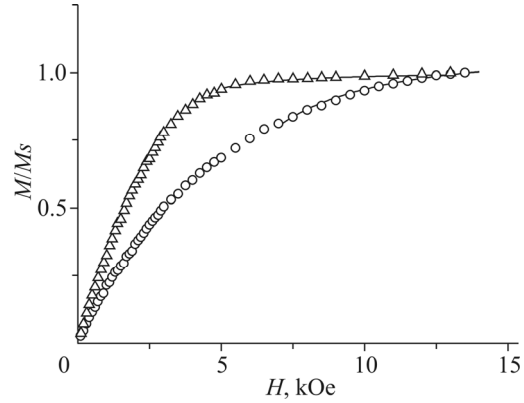


**Fig. 4.** Magnetization curves of bulk samples prepared by DC. The lines show the fittings of the high-field part of the magnetization curve by Akulov's law.

amorphous) are characterized by specific and almost composition independent Bloch constant  $B_i$  and local anisotropy field  $a_i H_{ai}$  values, the following system of equations can be written for heterophase alloy powders:

$$\begin{cases} x_{\text{hcp}} + x_{\text{fcc}} + x_A = 1 \\ B_1 x_{\text{hcp}} + B_2 x_{\text{fcc}} + B_3 x_A = B_{\text{eff}} \\ (a_1 H_{a1})^2 x_{\text{hcp}} + (a_2 H_{a2})^2 x_{\text{fcc}} + (a_3 H_{a3})^2 x_A = (a H_{a,\text{eff}})^2. \end{cases}$$

By solving this system of equations, one can determine the fractions of hcp, fcc, and amorphous phases in the studied powders and compacts based on Co(P) alloys [13]. The Table 1 summarizes the calculation data obtained for all

**TABLE 1.** Volume Fractions of hcp ( $x_{\text{hcp}}$ ), fcc ( $x_{\text{fcc}}$ ), and Amorphous ( $x_A$ ) Phases in the Studied Samples

Sample	$x_{\text{hcp}}$	$x_{\text{fcc}}$	$x_A$
Powder Co <sub>88</sub> P <sub>12</sub>	0.02	0.38	0.60
Compact Co <sub>88</sub> P <sub>12</sub> (CP, $P = 8$ atm)	0.02	0.35	0.63
Powder (Co <sub>88</sub> P <sub>12</sub> ) <sub>80</sub> Cu <sub>20</sub>	0.07	0.28	0.65
Compact (Co <sub>88</sub> P <sub>12</sub> ) <sub>80</sub> Cu <sub>20</sub> (DC)	0.13	0.26	0.61
Compact (Co <sub>88</sub> P <sub>12</sub> ) <sub>80</sub> Cu <sub>20</sub> (CP, $P = 5$ atm)	0.06	0.16	0.78
Compact (Co <sub>88</sub> P <sub>12</sub> ) <sub>80</sub> Cu <sub>20</sub> (CP, $P = 8$ atm)	0.07	0.15	0.78
Powder (Co <sub>88</sub> P <sub>12</sub> ) <sub>60</sub> Cu <sub>40</sub>	0.18	0.29	0.53
Compact (Co <sub>88</sub> P <sub>12</sub> ) <sub>60</sub> Cu <sub>40</sub> (DC)	0.22	0.24	0.54
Powder (Co <sub>88</sub> P <sub>12</sub> ) <sub>50</sub> Cu <sub>50</sub>	0.16	0.33	0.51
Compact (Co <sub>88</sub> P <sub>12</sub> ) <sub>50</sub> Cu <sub>50</sub> (DC)	0.17	0.34	0.51
Compact (Co <sub>88</sub> P <sub>12</sub> ) <sub>50</sub> Cu <sub>50</sub> (CP, $P = 5$ atm)	0.03	0.18	0.79
Compact (Co <sub>88</sub> P <sub>12</sub> ) <sub>50</sub> Cu <sub>50</sub> (CP, $P = 8$ atm)	0.08	0.14	0.78
Powder (Co <sub>88</sub> P <sub>12</sub> ) <sub>30</sub> Cu <sub>70</sub>	0.16	0.31	0.53
Compact (Co <sub>88</sub> P <sub>12</sub> ) <sub>30</sub> Cu <sub>70</sub> (DC)	0.16	0.32	0.52
Powder (Co <sub>95</sub> P <sub>5</sub> ) <sub>50</sub> Cu <sub>50</sub>	0.62	0.36	0.02
Compact (Co <sub>95</sub> P <sub>5</sub> ) <sub>50</sub> Cu <sub>50</sub> (DC)	0.78	0.21	0.01

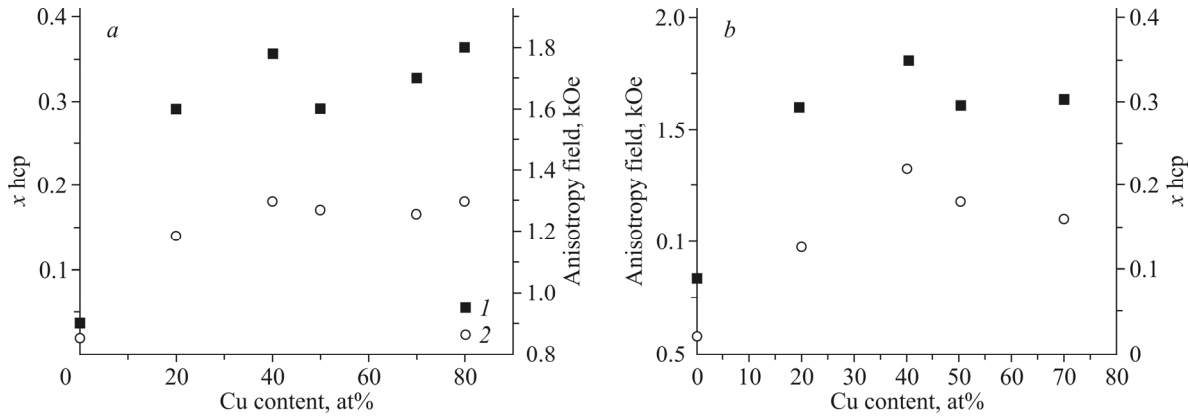


**Fig. 5.** Local anisotropy field (1) and fraction of the hcp phase as functions of copper content (2) for initial powders (a) and bulk samples prepared by dynamic compaction (b).

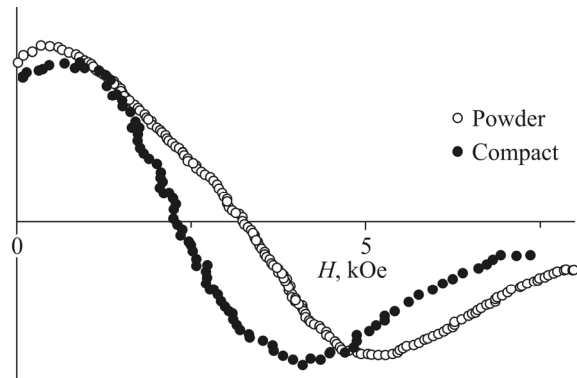


**Fig. 6.** Typical FMR spectra of initial powder  $\text{Co}_{88}\text{P}_{12}/\text{Cu}$  and the bulk sample prepared by dynamic compaction.

series of samples. The obtained results with the above NMR data provided that the amorphous core of composite particles has a fcc type immediate environment.

Dynamic compaction increases the fraction of the hcp phase in the particles with both crystal ( $\text{Co}_{95}\text{P}_5$ ) and amorphous ( $\text{Co}_{88}\text{P}_{12}$ ) cores. Apparently, some atoms have time to rearrange into the cobalt  $\alpha$ -phase (equilibrium phase at room temperature) when the sample is quenched after the shock wave. No such rearrangement is observed upon cold pressing. Thus, the proposed method of magnetic phase analysis provides a quantitative estimation of hcp, fcc, and amorphous phase contents in the sample and revealed the dependence of the local anisotropy field on the copper shell thickness. Fig. 5 shows the local anisotropy field and the fraction of the hcp phase as functions of the copper content in initial powders and compacts prepared by dynamic compaction. As can be seen, the concentration dependences  $H_a$  and  $X_{hcp}$  are qualitatively similar, i.e. the content of the phase with the highest  $H_a$  value ( $H_a$  is  $\sim 1$  kOe and  $\sim 10$  kOe for fcc and hcp phases, respectively) determines also the anisotropy of the whole sample.

It was established that the FMR line narrows as a result of the shock-wave loading of composite particles (Fig. 6). This narrowing correlates with the increase of the hcp phase amount during compaction. Indeed, the FMR line width is  $\Delta H_{\text{FMR}} \sim 5.4$  kOe for amorphous powders  $\text{Co}(\text{P})/\text{Cu}$ ,  $\sim 3.8$  kOe for compacts  $\Delta H_{\text{FMR}}$ , and  $\Delta H_{\text{FMR}} \sim 1$  kOe for crystalline powders  $\text{Co}_{95}\text{P}_5$  with a hcp lattice [9].

## CONCLUSIONS

Bulk composite materials  $\text{Co}(\text{P})/\text{Cu}$  preserving the core–shell structure of initial composite particles were prepared by dynamic compacting and uniaxial pressing. It was established that alloys  $\text{Co}_{88}\text{P}_{12}$  and  $\text{Co}_{95}\text{P}_5$  are heterophase systems

(a mixture of fcc and hcp short-range order phases) both in the initial powders and in the compacts. The shock wave loading during the compaction changes the ratio of atoms with hcp and fcc symmetries of immediate environment. The phase composition of the powders and compacts was determined quantitatively by magnetic phase analysis. It was established that the FMR line width is diminished as a result of shock-wave loading during compaction since the number of atoms with the hcp type nearest environment increases. The saturation magnetization and coercive force ( $H_C \sim 200$  Oe) values remain virtually unchanged after compaction.

## ACKNOWLEDGMENTS

The authors acknowledge the Krasnoyarsk Regional Center of Research Equipment of Federal Research Center “Krasnoyarsk Science Center SB RAS” for providing the measurement equipment.

## FUNDING

The study was supported by RFBR, the Government of the Krasnoyarsk Region, and the Krasnoyarsk Regional Science Foundation within project No. 20-43-240003.

## CONFLICT OF INTERESTS

The authors declare that they have no conflict of interests.

## REFERENCES

1. P. Vojtanik. *J. Magn. Magn. Mater.*, **2006**, *304*, 159.
2. A. Inoue, B. Shen, and A. Takeuchi. *Mater. Sci. Eng., A*, **2006**, *441*, 18.
3. N. P. Ljakishev and M. I. Alymov. *Ross. Nanotekhnol.*, **2006**, *1*(1–2), 71.
4. R. A. Andrievsky and A. V. Ragulya. *Nanostrukt. Mater.* (Nanostruct. Mater.) [in Russian]. Akademiya: Moscow, **2005**.
5. R. Z. Valiev, R. K. Islamgaliev, and I.V. Alexandrov. *Prog. Mater. Sci.*, **2000**, *45*, 103.
6. A. I. Gusev. *Nanomater., Nanostrukt., Nanotekhnol.* (Nanomater., Nanostruct., Nanotechnol.) [in Russian]. Fizmatlit: Moscow, **2007**.
7. A. A. Rempel. *Usp. Khim.*, **2007**, *76*(5), 474.
8. R. S. Iskhakov, E. A. Denisova, and A. A. Lepeshev. *Pis'ma Zh. Eksp. Teor. Fiz.*, **1995**, *62*, 548.
9. R. S. Iskhakov, L. A. Chekanova, and E. A. Denisova. *Fiz. Tverd. Tela*, **1999**, *41*(3), 464.
10. R. S. Iskhakov, E. A. Denisova, S. V. Komogortsev, A. D. Balaev, and G. N. Bondarenko. *J. Optoelectron. Adv. Mater.*, **2008**, *10*, 1043.
11. R. S. Iskhakov, L. A. Kuzovnikova, S. V. Komogortsev, E. A. Denisova, V. K. Mal'tsev, and G. N. Bondarenko. *Chem. Sustainable Dev.*, **2005**, *13*, 209.
12. R. S. Iskhakov, V. A. Ignatchenko, S. V. Komogortsev, and A. D. Balaev. *JETP Lett.*, **2003**, *78*, 646.
13. L. A. Chekanova, E. A. Denisova, S. V. Komogortsev, R. S. Iskhakov, and O. A. Goncharova. *Phys. Met. Metallogr.*, **2013**, *114*(2), 122.
14. V. V. Serikov, N. M. Kleinerman, and O. A. Golovnja. *Phys. Met. Metallogr.*, **2017**, *118*(11), 1040.
15. O. V. Lapina. *Catal. Today*, **2017**, *285*, 179.
16. A. S. Andreev, O. B. Lapina, J. B. d'Espinose de Lacaillerie, and A. A. Khassin. *J. Struct. Chem.*, **2013**, *54*, S102–S110.
17. J. Durand and M. F. Lapierre. *J. Phys. F: Met. Phys.*, **1976**, *6*(4), 1185.
18. L. A. Kuzovnikova, R. S. Iskhakov, S. V. Komogortsev, E. A. Denisova, A. D. Balaev, V. K. Mal'tsev, and G. N. Bondarenko. *Tech. Phys. Lett.*, **2004**, *30*(1), 60.
19. A. A. Shmyreva, V. V. Matveev, and G. Yu. Yurkov. *Int. J. Nanotechnol.*, **2016**, *13*, 126.